# First-principles study for low-spin $LaCoO_3$ with a structurally consistent Hubbard $U$

Han Hsu, Koichiro Umemoto, Matteo Cococcioni, and Renata Wentzcovitch
*Department of Chemical Engineering and Materials Science, University of Minnesota, Minneapolis, Minnesota 55455, USA*
(Received 11 October 2008; revised manuscript received 8 January 2009; published 31 March 2009)

In this paper, we use the local density approximation+Hubbard $U$ method to calculate the structural and electronic properties of low-spin $LaCoO_3$. The Hubbard $U$ is obtained by first principles and consistent with each fully optimized atomic structure at different pressures. With structurally consistent $U$, the fully optimized atomic structure agrees with experimental data better than the calculations with fixed or vanishing $U$. A discussion on how the Hubbard $U$ affects the electronic and atomic structures of $LaCoO_3$ is also given.

DOI: 10.1103/PhysRevB.79.125124 PACS number(s): 61.66.Fn, 64.30.Jk, 71.15.Mb, 71.20.Ps

## I. INTRODUCTION

Interest toward perovskite cobaltites, especially $LaCoO_3$, can be dated back to decades ago because of their unique properties, such as the occurrence of non-metal-to-metal transition and spin-state transition.[1–3] At low temperature, $LaCoO_3$ is nonmetal with vanishing magnetization, i.e., the $Co^{3+}$ cations are in the low-spin (LS) ($S=0$) state. As the temperature is raised to about 100 K, $LaCoO_3$ undergoes a crossover from the nonmagnetic to a magnetic state. Such a crossover transition was first suggested to be from the low-spin state to a high-spin (HS) ($S=2$) state, as reviewed in Refs. 1–3. Later, several density functional theory (DFT)-based calculations[4–9] indicated that intermediate-spin (IS) ($S=1$) state of $Co^{3+}$ can stably exist and is involved in the spin-state crossover transition around 100 K. Much effort has been devoted to sharpen the evidences in support of or to question the existence of IS state and its role in spin-state transition ever since[10–23] but there still remain controversy. On the theoretical side, calculations based on $CoO_6$ cluster models showed that it is difficult to stabilize the IS state.[20–22] Also, DFT-based calculations with the same method do not entirely agree with each other on this issue. Both pure IS state[7] and LS-HS mixture[8] have been attributed to cause the spin-state transition at around 100 K.

In addition to temperature, pressure can also induce spin-state transition and lattice distortions in $LaCoO_3$.[24–27] For example, at room temperature, the anomalous change in structural parameters at a pressure of about 4 GPa was attributed to the IS-to-LS transition, as proposed in Ref. 24.

As shown in the experimental works mentioned above, accompanying with thermal- or pressure-induced spin-state transition, anomalous variations in magnetic susceptibility, thermal expansion, bulk modulus, and structural parameters with temperature[10–23] or pressure[24–27] can occur. Although these anomalies have been used as signatures of the occurrence of spin-state transition, the *normal* behavior of LS $LaCoO_3$ structural parameters has not been clarified.

So far, in most DFT-based calculations for $LaCoO_3$,[4–9] the lattice structures are adopted from neutron or x-ray diffraction experiments (see Refs. 16 and 24 for example). The electronic structures and spin states at different pressures and temperatures are calculated using the experimental lattice structures measured at the corresponding pressure and temperature. To further understand the properties of $LaCoO_3$ at different conditions, an *ab initio* calculation starting with the determination of $LaCoO_3$ lattice structure is of interest. A predictive study of LS $LaCoO_3$ would be a good starting point.

It is known that the local density approximation (LDA) and generalized-gradient approximation (GGA) could give incorrect result for transition-metal oxide systems. For example, LDA and GGA produce metallic ground state for LS $LaCoO_3$, as shall be shown later, while LS $LaCoO_3$ is insulating at low temperature.[1–3,14,19,28–30] Corrections that account for the strong correlation among the electrons at the Co sites can be made by using the so-called DFT+$U$ approach. In this approach, the usual approximate DFT energy functional (LDA or GGA) is corrected by an additional term that depends on the effective on-site electron-electron interaction in a manner similar to the $U$ term in the Hubbard model. Such DFT+$U$ method has been successfully used in the calculations of many transition-metal oxides.[31–33] In many previous DFT+$U$ calculations of $LaCoO_3$, the values of Hubbard $U$ are chosen to be constant[4–9] regardless of the spin state of $Co^{3+}$ or the volume of unit cell. However, it has been demonstrated that the Hubbard $U$ value can vary with those quantities in the same material.[32,33] Therefore, to get more accurate results for LS $LaCoO_3$, a structure-dependent $U$ is necessary.

In this paper, we compare the atomic and electronic structures of LS $LaCoO_3$ obtained from several methods: LDA, GGA, and LDA+$U$ with different choices of $U$, including fixed and structure-dependent $U$. In Sec. II, a discussion for the determination of structurally consistent $U$ is given. Comparison for the results obtained from different methods is made in Sec. III. Concluding remarks are offered in Sec. IV.

## II. STRUCTURALLY CONSISTENT HUBBARD $U$ AND COMPUTATION

For a given structure, the functional of total energy $E$ in LDA+$U$ method is written as

$$E = E_{\mathrm{LDA}} + \frac{U}{2}\sum_{I,\sigma} \mathrm{Tr}[\mathbf{n}^{I\sigma}(1-\mathbf{n}^{I\sigma})], \tag{1}$$

where $E_{\mathrm{LDA}}$ is the LDA ground-state energy of the structure and $\mathbf{n}^{I\sigma}$ is the occupation matrix of the atomic site $I$ with spin $\sigma$. The Hubbard $U$ of this given structure can be calculated

 

based on linear response theory, as detailed in Ref. 33. Briefly speaking, this procedure starts with computing the LDA ground state of this given structure. With the LDA ground state, the occupation $\mathbf{n}^{I\sigma}$ at each Hubbard site $I$ can be determined accordingly. The next step is to apply perturbations to the potential localized at Hubbard site $I$. The perturbed states lead to different occupations with respect to the unperturbed one. The linear response of occupation $\mathbf{n}^{I\sigma}$ to the local potential shift is used to determine the Hubbard $U$. Within this scheme, a supercell approach is usually adopted to simulate a single Hubbard site being perturbed in an infinite crystal.[33] For LS $LaCoO_3$, we have tested the Hubbard $U$'s obtained using rhombohedral unit cell containing 10 atoms (2 Co atoms), hexagonal cell containing 30 atoms (6 Co atoms), and $2\times2\times2$ supercell containing 80 atoms (16 Co atoms). The results given by hexagonal cell and $2\times2\times2$ supercell are within about 0.05 eV. In this paper, all the Hubbard $U$'s are computed using hexagonal cells.

The calculation of structurally consistent Hubbard $U$ is based on an iterative procedure that starts with a structure optimization within LDA ($U=0$). The $U$ computed for this LDA equilibrium structure is referred to as $U_o$. Then, an LDA+$U$ structural optimization is performed with $U=U_o$, and this generally leads to a configuration different from the LDA-optimized structure. A different calculation for the $U$ parameter is performed with the present structure, and this present $U$ is used in the next structure optimization. This cyclic procedure is stopped when the convergence of $U$ and structural parameters is achieved. Typically, after three to four iterations, the presently obtained $U$ can be within 0.03 eV from the previous $U$, and the atomic structure essentially remains the same. This structurally consistent $U$ is referred to as $U_{sc}$ in this paper.

The pressure $P$ is determined by the negative derivative of total energy with respect to volume,

$$P = -\frac{\partial E_{\mathrm{LDA}}}{\partial V} - \frac{\partial U}{2\,\partial V}\sum_{I,\sigma}\mathrm{Tr}[\mathbf{n}^{I\sigma}(1-\mathbf{n}^{I\sigma})] - \frac{U}{2}\sum_{I,\sigma}\frac{\partial}{\partial V}\mathrm{Tr}[\mathbf{n}^{I\sigma}(1-\mathbf{n}^{I\sigma})]. \quad (2)$$

Based on this equation, pressure depends on the volume/structure dependence of $U$. If $U$ is chosen to be a constant, then the effect from the second term (proportional to $\partial U/\partial V$) is missed. A discussion on how the choice of $U$ affects $P$ will be given in Sec. III.

The computations are carried out using the QUANTUM-ESPRESSO package.[34] The pseudopotentials are generated by the method of Vanderbilt.[35] The valence electronic configurations used are $5s^25p^65d^16s^16p^14f^0$, $3s^23p^63d^{6.5}4s^24p^0$, and $2s^22p^4$ for La, Co, and O, respectively. Core radii are $r_s=r_p=r_d=2.2$ a.u. and $r_f=1.7$ a.u. for La, $r_s=r_p=r_d=1.8$ a.u. for Co, and $r_s=r_p=1.4$ a.u. for O. The energy cutoff is 64 Ry for the wave function and 640 Ry for the charge density. For Brillouin-zone sampling, $8\times8\times8$ $k$-point mesh is used. Structural optimization is performed using variable cell shape molecular dynamics.[36] When the interatomic forces are smaller than $10^{-4}$ Ry/a.u., the relaxation is terminated. The compression curves are fitted to the third-order Birch-Murnaghan equation.

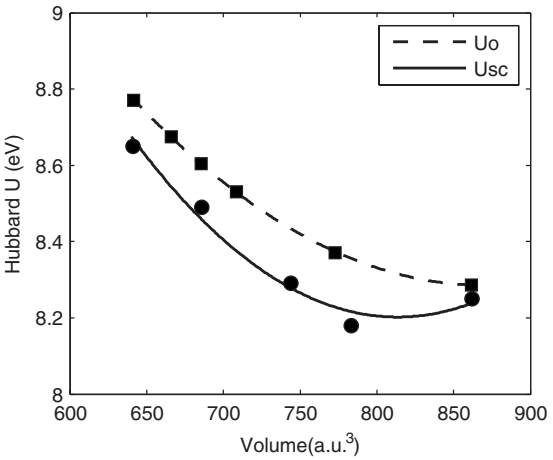


FIG. 1. Hubbard $U$ as a function of LS $LaCoO_3$ rhombohedral unit-cell volume $V$. The Hubbard $U$ of the LDA-relaxed structure is referred to as $U_o$ (dashed line), and the structurally consistent $U$ (see text) is referred to as $U_{sc}$ (solid line). While $U_o$ decreases with $V$, $U_{sc}$ has a minimum of 8.20 eV at $V=814$ a.u.$^3$. The different volume dependence affects the estimate of pressure, as later shown in Fig. 3.

## III. RESULTS AND DISCUSSION

We first show the dependence of $U_o$, the Hubbard $U$ of the LDA-relaxed LS $LaCoO_3$, and $U_{sc}$, the structurally consistent Hubbard $U$ of LS $LaCoO_3$, on the unit-cell volume ($V$) in Fig. 1. The difference between $U_o$ and $U_{sc}$ is not very large. The maximum of $U_o-U_{sc}$ is 0.16 eV occurring at $V=731$ a.u.$^3$. Their derivatives with respect to $V$, however, are very different. For the volume range considered in this paper, $U_o$ monotonically decreases with $V$, while $U_{sc}$ decreases to a minimum of 8.20 eV at $V=814$ a.u.$^3$ and then increases. For larger volumes, $U_{sc}$ seems to approach $U_o$. Such difference in volume dependence affects the calculation of pressure, as can be seen from Eq. (2).

In Fig. 2, the total energies $E$ as functions of unit-cell volume $V$ obtained from different choices of the Hubbard $U$ are plotted, including volume-dependent $U_o$ and $U_{sc}$, and fixed $U=8.33$ eV (average of $U_{sc}$) and $U=8.46$ eV (average of $U_o$). For the cases of two fixed $U$'s, the two corresponding $E(V)$ curves have very similar shape, and their minima occur at almost the same volume. We can thus expect these two fixed values of $U$ to give almost identical volume-pressure relations. On the other hand, the shapes of the $E(V)$ curves given by the volume-dependent $U_o$ and $U_{sc}$ are different from the fixed $U$ results and also from each other. At smaller volumes ($V<675$ a.u.$^3$) where $\partial U_o/\partial V\approx\partial U_{sc}/\partial V$, the corresponding $E(V)$ curves have almost the same slope. Around $V=731$ a.u.$^3$ where $U_o-U_{sc}$ has a maximum, the corresponding $E(V)$ curves also differ the most. At large $V$s where $U_o$ approaches $U_{sc}$, the corresponding $E(V)$ curves also approach each other.

Next, we demonstrate how the structural properties of $LaCoO_3$ and their response to pressure are affected by dif-

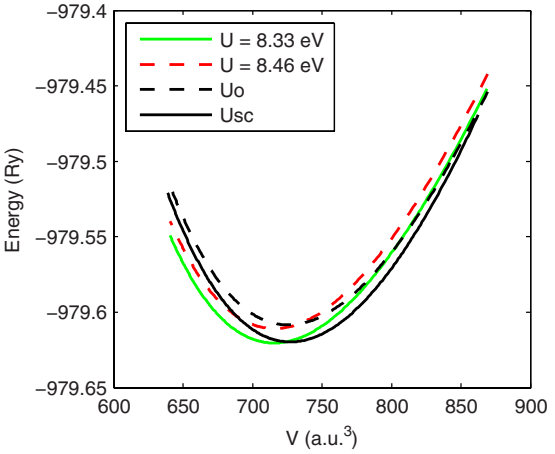


FIG. 2. (Color online) Total energies $E$ as functions of LS $LaCoO_3$ unit-cell volume $V$ obtained from different choices of Hubbard $U$: volume-dependent $U_o$, $U_{sc}$, and fixed $U=8.46$ eV (average of $U_o$) and $U=8.33$ eV (average of $U_{sc}$). The $E(V)$ curves obtained from the two fixed $U$'s have very similar shape, and the $E(V)$ curves obtained from the volume-dependent $U_o$ and $U_{sc}$ have different shapes.

ferent choices of the Hubbard $U$. The zero-temperature volumes and structural parameters of LS $LaCoO_3$ for pressures ranging from −28 to 34 GPa determined by LDA, GGA, and LDA+$U$ with different choices of $U$ are shown in Figs. 3–5. Two sets of experimental data are presented along with our calculation for comparison. The orange squares are the data taken under ambient pressure ($10^{-4}$ GPa) at temperature $T=5$ K,[16] and the green triangles are the data taken at room temperature ($T=298$ K) with pressures ranging from $10^{-4}$ to 8 GPa.[24] Due to the spin excitation caused by temperature and the pressure-induced spin-state transition, it can be expected that the calculated structural parameters and the ones measured at $T=298$ K can vary with pressure in different manners.

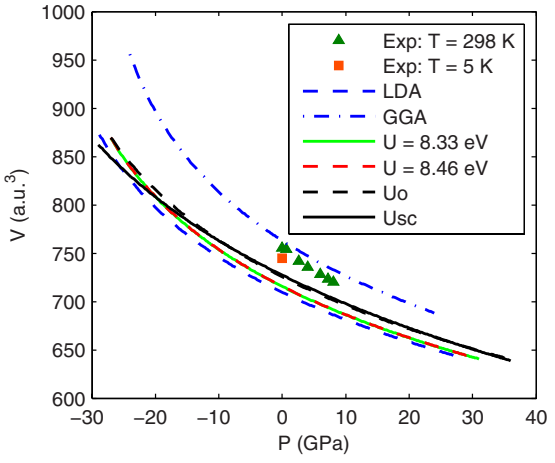


FIG. 3. (Color online) Calculated zero-temperature volume at different pressures. At $P=0$ GPa, the volume given by LDA+$U$ with $U_{sc}$ agrees with the experimental data taken at $T=5$ K, $P=10^{-4}$ GPa (orange square) (Ref. 16) better than other calculated results. Experimental data taken at room temperature (green triangles) (Ref. 24) are shown as a reference.

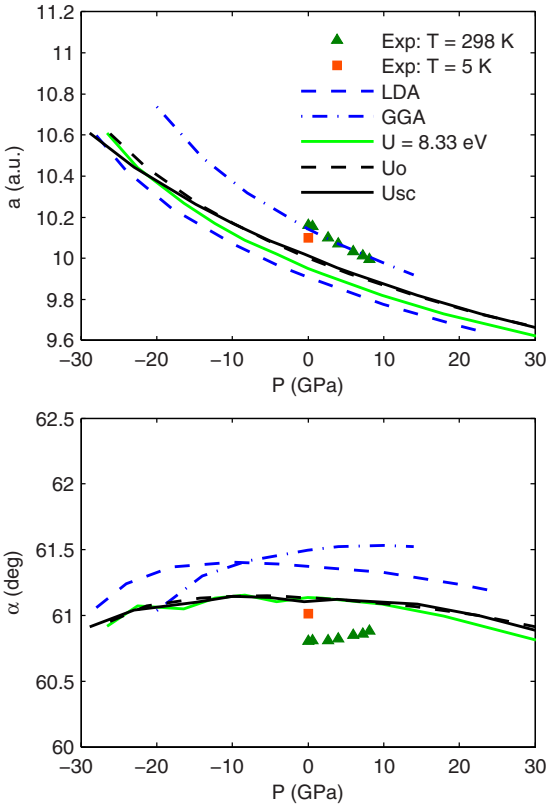


FIG. 4. (Color online) Lattice constant $a$ (top) and rhombohedral angle $\alpha$ (bottom) of LS $LaCoO_3$ at different pressures. At $P=0$ GPa, the results of LDA+$U$ with $U_{sc}$ agree best with the experimental data taken at $T=5$ K (Ref. 16). The discrepancy with respect to the $T=298$ K (Ref. 24) data is a signature of spin excitations.

In Fig. 3, the volume dependence on pressure is plotted. The zero-temperature equilibrium volumes (at $P=0$ GPa) given by different methods are listed in Table I. Compared with the experimental volume $V=745.1577$ a.u.$^3$ at $T=5$ K, LDA underestimates the equilibrium volume by 4.79% and GGA overestimates the volume by 2.39%. By applying $U$, the results get closer to the experimental value. Different choices of $U$ improve over LDA differently. The structurally consistent $U_{sc}$ improves the most and gives $V=727.2558$ a.u.$^3$ at $P=0$ GPa, underestimating the volume by 2.40%. The results with $U_{sc}$ are expected to be further improved with the inclusion of zero-point motion.

When $P\neq 0$, different choices of $U$ give different volume-pressure relations. In most of the pressure range (−25.6 to 34 GPa), LDA gives the smallest volume, and applying $U$ increases the volume. This suggests that GGA+$U$ may not be appropriate for $LaCoO_3$ structural optimization. It could overestimate volume more than GGA already does. The results obtained from the two fixed $U$'s ($U=8.33$ and 8.46 eV) are very similar because the value difference in $U$ is not large enough to cause significant difference in atomic and electronic structures, and the same volume dependence of fixed $U$ gives very similar pressure. This can also be seen from Fig. 2, where the $E(V)$ with $U=8.33$ eV is essentially the same as that with $U=8.46$ eV but just shifted vertically by 0.096 Ry. As to the cases of $U_o$ and $U_{sc}$, they give similar

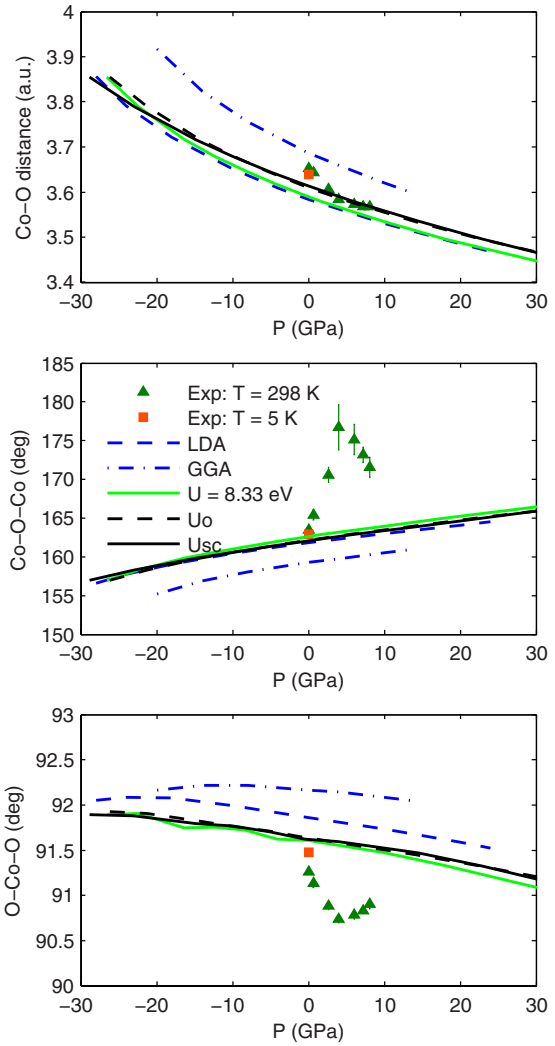


FIG. 5. (Color online) Structural parameters of $LaCoO_3$, Co-O distance (top), Co-O-Co bond angle (middle), and O-Co-O bond angle (bottom), at different pressures. At $P=0$ GPa, the results of LDA+$U$ with $U_{sc}$ agree best with the experimental data taken at $T=5$ K (Ref. 16). The discrepancy with respect to the $T=298$ K data (Ref. 24) is a signature of spin excitations.

volume-pressure relations for greater $P$'s (smaller $V$'s). When the lattice is expanded (at negative $P$), $U_{sc}$ gives a flatter $V$ vs $P$ curve. This is because with $U_{sc}$, expanding the lattice would be more difficult, which can be seen from the steeper $E(V)$ curve of $U_{sc}$ for larger volumes in Fig. 2.

Most experimental works show $LaCoO_3$ having rhombohedral unit cell ($R\bar{3}c$ symmetry) with ten atoms. Three parameters can be used to describe such type of structure: lattice constant $a$, rhombohedral angle $\alpha$ between lattice vectors, and the atomic coordinate $x$ of oxygen at the 6$e$ Wyckoff position. Another set of parameters can be used for structure description as well: Co-O distance, Co-O-Co bond angle, and O-Co-O bond angle. Instead of plotting $a$, $\alpha$, and $x$, we plot $a$, $\alpha$, and the parameters of $CoO_6$ octahedra for better understanding how the atomic structure responds to external pressure and Hubbard $U$. If $LaCoO_3$ were undistorted cubic perovskite, its $\alpha$, Co-O-Co, and O-Co-O bond angles would be 60°, 180°, and 90°, respectively.

TABLE I. Calculated 0 K volume (at $P=0$) and experimental 5 K volume (at $P=10^{-4}$ GPa) of LS $LaCoO_3$ rhombohedral unit cell. The result obtained by using LDA+$U$ method with $U_{sc}$, structurally consistent Hubbard $U$, agrees with experimental data better than other methods.

| | Volume (a.u.$^3$) | Deviation (%) |
|---|---|---|
| $T=5$ K (Ref. 16) | 745.1577 | 0 |
| LDA | 709.4681 | −4.79 |
| GGA | 762.9661 | 2.39 |
| $U=8.33$ eV | 715.5514 | −3.97 |
| $U=8.46$ eV | 715.6860 | −3.96 |
| $U_o$ | 725.5865 | −2.63 |
| $U_{sc}$ | 727.2558 | −2.40 |

In Fig. 4, lattice constant $a$ and rhombohedral angle $\alpha$ are plotted versus pressure. Similar to the compression curves in Fig. 3, LDA underestimates the lattice constant $a$ the most, GGA overestimates, and $U_{sc}$ gives the best result at $P=0$. For the rhombohedral angle $\alpha$, applying the Hubbard $U$ makes the LS $LoCoO_3$ less distorted from cubic perovskite ($\alpha=60°$). This also makes the LDA+$U$ results closer to the $T=5$ K data.

In Fig. 5, the Co-O distance, Co-O-Co, and O-Co-O bond angles are plotted versus pressure. The $T=298$ K structural parameters have a qualitatively different behavior from the calculated LS $LaCoO_3$ results. The main reason is that at

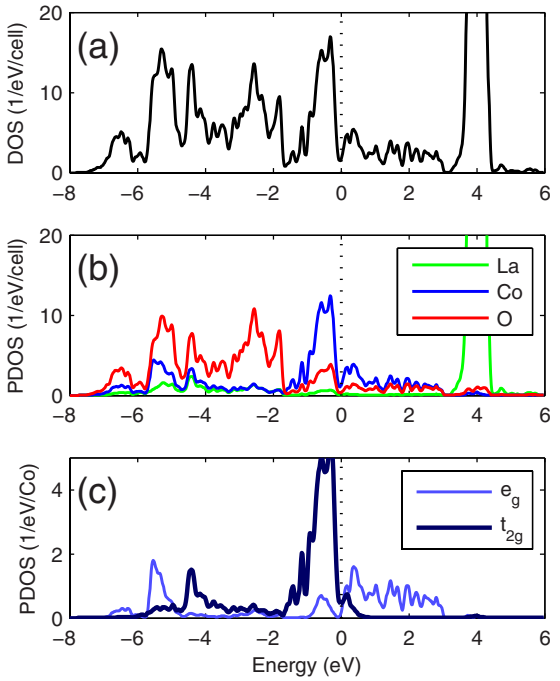


FIG. 6. (Color online) Total and partial densities of states of LS $LaCoO_3$ at $V=744.65$ a.u.$^3$ obtained using LDA (experimental equilibrium $V=745.16$ a.u.$^3$). (a) Total density of states; (b) partial density of states of different atoms; and (c) partial density of states of $e_g$ and $t_{2g}$ states. LDA gives metallic $LaCoO_3$ at low temperature. The occupation of $t_{2g}$ state is 5.66/Co.

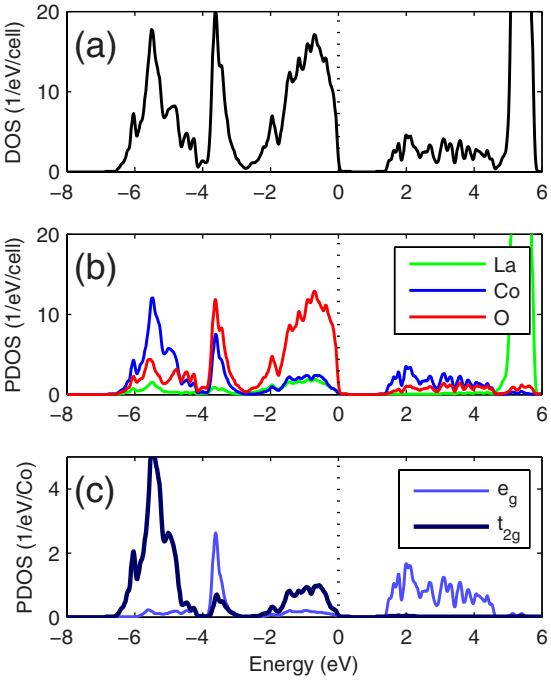


FIG. 7. (Color online) Total and partial densities of states of LS $LaCoO_3$ at $V=744.13$ a.u.$^3$ obtained using LDA+$U$ (experimental equilibrium $V=745.16$ a.u.$^3$). (a) Total density of states; (b) partial density of states of different atoms; and (c) partial density of states of $e_g$ and $t_{2g}$ states. Applying $U$ opens an indirect gap of 1.43 eV. The occupation of $t_{2g}$ state is 5.91/Co.

room temperature, $LaCoO_3$ is no longer in the LS state. We can also notice that when LS $LaCoO_3$ is compressed, the Co-O-Co and O-Co-O angles are closer to the cubic perovskite values (180° and 90°).

To further understand how LDA+$U$ (especially with $U_{sc}$) improves over LDA, we compare the density of states (DOS), maximally localized Wannier functions (MLWFs), charge density, and structural parameters of LS $LaCoO_3$ obtained from LDA and LDA+$U_{sc}$ at around the experimental equilibrium volume (745.16 a.u.$^3$). In the calculations, the unit-cell volumes are 744.64 and 744.13 a.u.$^3$ for LDA and LDA+$U_{sc}$, respectively.

Figures 6 and 7 show the density of states and partial density of states (PDOS) obtained from LDA and LDA+$U$ (with $U_{sc}$), respectively. In PDOS, the projections of the wave function on the localized states at each atomic site are shown, including the projection on the five 3$d$ states at the Co site—two $e_g$ states ($d_{3z^2-r^2}, d_{x^2-y^2}$) and three $t_{2g}$ states ($d_{xy}, d_{yz}, d_{zx}$), where the $x$, $y$, and $z$ axes are closely aligned

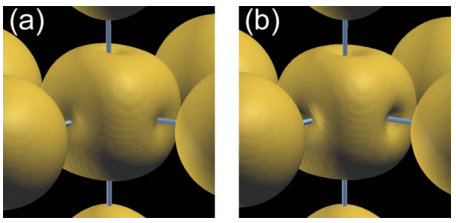


FIG. 8. (Color online) Charge density of LS $LaCoO_3$ around Co given by (a) LDA at $V=744.65$ a.u.$^3$ and (b) LDA+$U$ at $V=744.13$ a.u.$^3$ Co is placed at the center and surrounded by six O sites. The charge density on the Co site given by LDA+$U$ has deeper dimples and a more cubiclike shape. This shows a more confined and $t_{2g}$-like charge density. The isosurface value is 0.09.

with the Co-O axes in $CoO_6$ octahedra. Similar to other calculations,[4,6] LDA gives metallic $LaCoO_3$, and LDA+$U$ opens a gap. In our calculation, the gap is 1.43 eV, and it is an indirect gap. The top of the valence band occurs at the $\Gamma(000)$ point, and the bottom of the conduction band occurs at the $F(\frac{1}{2}\frac{1}{2}0)$ point. The calculated gap is greater than the results of optical conductivity measurements, from which an indirect gap between 0.1 and 1 eV was estimated,[28–30,37] and also greater than the results of ultraviolet photoemission spectroscopy (UPS) spectrum, from which a gap of 0.6 eV was estimated.[38] In addition to opening a gap, the Hubbard $U$ also causes the valence band separating into three subgroups, as can be seen in Fig. 7(a). The subgroup right below $E_F$ is mainly formed by O 2$p$ states, and most of the $t_{2g}$ states are shifted to the bottom of the band. The grouping feature of the valence band and the corresponding DOS peaks agree with the x-ray photoemission spectroscopy (XPS) spectra taken at $T=80$ K.[39,40] At this temperature, most Co atoms are in the LS state. The peaks of the XPS spectrum shown in Ref. 39 occur at −1.3, −3.4, and −5.5 eV, and the energy resolution was approximately 0.9 eV. Our calculated LDA+$U$ DOS peaks occur at −0.7, −3.6, and −5.5 eV. The full width at half maximum (FWHM) of these peaks are 1.4, 0.4, and 0.5 eV, respectively. On the contrary, the valence band in LDA does not show evident grouping feature. In this sense, LDA+$U$ gives a more accurate description for the electronic structure than LDA does.

One can notice that in both LDA and LDA+$U$ cases, the projection on $e_g$ states are nonvanishing. In LDA+$U$, the PDOS peak of $e_g$ states occurs at −3.6 eV—same as the PDOS peak of O 2$p$. In LDA, however, no peak of $e_g$ and O 2$p$ occurs at the same energy. This suggests that in LDA+$U$, bonding states between Co and O are formed. More detailed discussions on the bonding states will be given later.

TABLE II. Structural parameters of LS $LaCoO_3$ at $V\approx745$ a.u.$^3$. The result obtained from $U_{sc}$ is closer to the experimental data.

| | Volume (a.u.$^3$) | $a$ (a.u.) | $\alpha$ (deg) | Co-O (a.u.) | Co-O-Co (deg) | O-Co-O (deg) |
|---|---|---|---|---|---|---|
| $T=5$ K (Ref. 16) | 745.1577 | 10.1001 | 61.01 | 3.6383 | 162.93 | 91.48 |
| LDA | 744.6498 | 10.0691 | 61.40 | 3.6507 | 160.41 | 91.99 |
| $U_{sc}$ | 744.1255 | 10.0863 | 61.14 | 3.6445 | 161.36 | 91.70 |

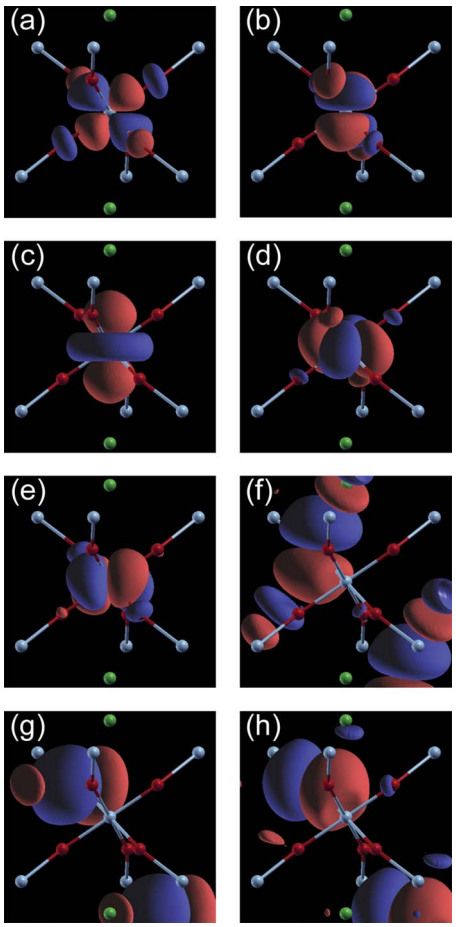


FIG. 9. (Color online) MLWFs of LS $LaCoO_3$ at $V=744.65$ a.u.$^3$ given by LDA. Green, light blue, and red spheres represent La, Co, and O sites, respectively. The isosurface values are $\pm 0.60$. [(a)–(e)] MLWFs associated with the Co $3d$ band; [(f)–(h)] MLWFs associated with the O $2p$ band. In order to see how the O $2p$ electrons bond with the atoms in the adjacent unit cell, each O $2p$ MLWF in panels (f)–(h) is duplicated and plotted at the equivalent atomic site in the adjacent cell.

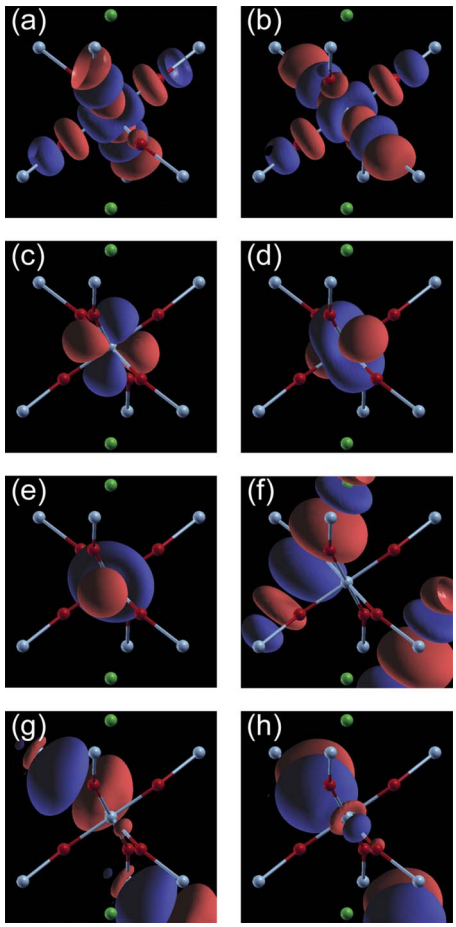


FIG. 10. (Color online) MLWFs of LS $LaCoO_3$ at $V=744.13$ a.u.$^3$ given by LDA+$U_{sc}$. Green, light blue, and red spheres represent La, Co, and O sites, respectively. The isosurface values are $\pm 0.60$. [(a)–(e)] MLWFs associated with the Co $3d$ band; [(f)–(h)] MLWFs associated with the O $2p$ band. In order to see how the O $2p$ electrons bond with the atoms in the adjacent unit cell, each O $2p$ MLWF in panels (f)–(h) is duplicated and plotted at the equivalent atomic site in the adjacent cell.

Applying the Hubbard $U$ also makes the occupied states more $t_{2g}$-like. By integrating PDOS over energy, the occupation of $t_{2g}$ state is 5.66/Co in the LDA case and 5.91/Co in the LDA+$U$ case. The charge density shown in Fig. 8 is consistent with this. The LDA and LDA+$U$ charge densities are plotted in panels (a) and (b), respectively. In both panels, Co site is placed at the center of the picture surrounded by six O sites. The deeper dimples and the more cubic shape of LDA+$U$ charge density indicate that the occupied states have a more pronounced $t_{2g}$ character. The Co-O distance also becomes smaller in the presence of the Hubbard $U$, as shown in Table II. Smaller Co-O distance in LDA+$U$ makes $LaCoO_3$ less distorted. A quantity, Goldschmidt tolerance factor $t \equiv \langle \text{La-O} \rangle / \sqrt{2} \langle \text{Co-O} \rangle$, where $\langle \text{La-O} \rangle$ and $\langle \text{Co-O} \rangle$ are the average La-O and Co-O distances, can be used to analyze the distortion of perovskite structures. For cubic perovskite, $t=1$; for rhombohedrally compressed perovskite such as $LaCoO_3$, $t<1$. As mentioned above, LDA+$U$ gives smaller $\langle \text{Co-O} \rangle$, and the tolerance factor increases toward $t=1$, the value in cubic perovskite. Indeed, the Co-O-Co and O-Co-O bond angles are closer to 180° and 90° in the LDA+$U$ case.

Information about the orbitals and the formation of bonding or antibonding states can be obtained by plotting MLWFs.[41,42] The MLWFs of LS $LaCoO_3$ with $V \approx 745$ a.u.$^3$ are plotted in Figs. 9 and 10 for LDA and LDA+$U_{sc}$, respectively. All these MLWFs are constructed from the energy band formed by Co $3d$ and O $2p$ electrons. In both figures, panels (a)–(e) show the MLWFs associated with the Co $3d$ band, and panels (f)–(h) show the MLWFs associated with the O $2p$ band. In order to see how the O $2p$ electrons bond with atoms in the adjacent unit cell, each O $2p$ MLWF is duplicated and plotted at the equivalent O site in one of the adjacent cells. The calculation of MLWFs is performed using WANNIER90.[43] The convergence of the total spread of MLWFs is up to $10^{-7}$ Å$^2$, and the spread of each MLWF is smaller than 1.5 Å$^2$.

In the LDA case (Fig. 9), its Co $3d$ MLWFs are not exactly $e_g$ and $t_{2g}$ states. However, similar to the $e_g$ and $t_{2g}$ states in cubic perovskite, these five Co $3d$ MLWFs can still be divided into two subgroups: the ones mostly pointing to-

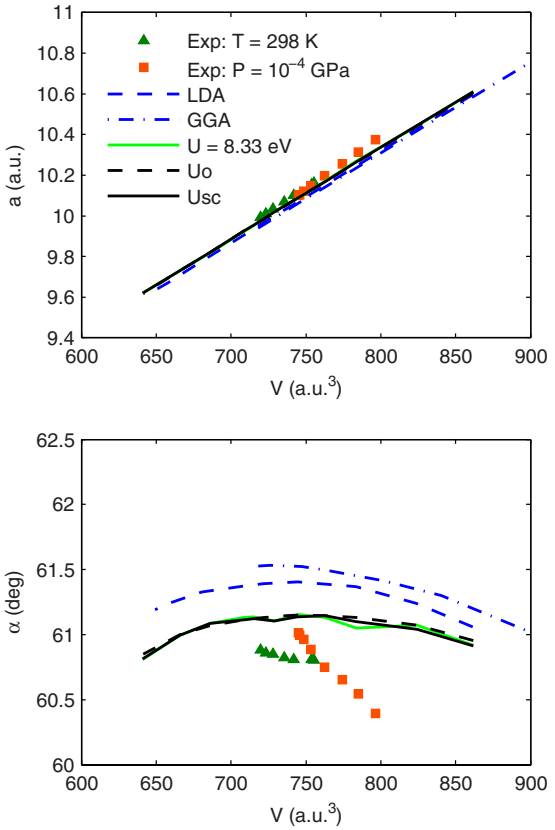


FIG. 11. (Color online) Lattice constant $a$ (top) and rhombohedral angle $\alpha$ (bottom) of LS $LaCoO_3$ unit cell as functions of unit-cell volume $V$. At $V=745$ a.u.$^3$, the results of LDA+$U$ agree with the experimental data taken at $T=5$ K, $P=10^{-4}$ GPa (Ref. 16) better than LDA. The discrepancy with respect to experimental data (Refs. 16 and 24) is a signature of spin excitations.

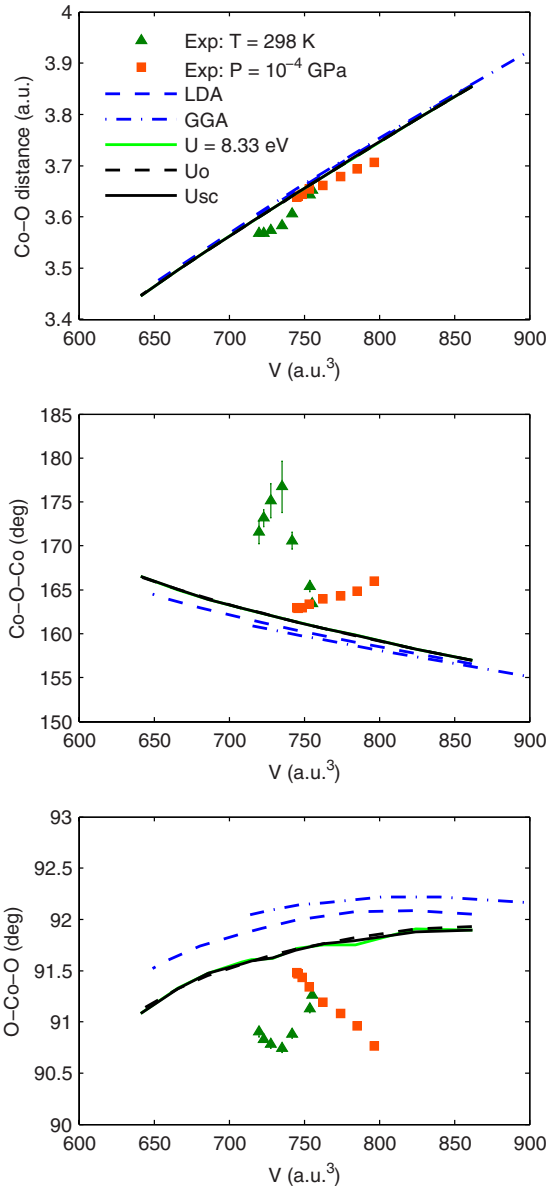


FIG. 12. (Color online) Structural parameters of $LaCoO_3$, Co-O distance (top), Co-O-Co bond angle (middle), and O-Co-O bond angle (bottom), as a function of unit-cell volume $V$. At $V=745$ a.u.$^3$, the results of LDA+$U$ agree with the experimental data taken at $T=5$ K, $P=10^{-4}$ GPa (Ref. 16) better than LDA. The discrepancy with respect to the experimental data (Refs. 16 and 24) is a signature of spin excitations.

ward the O sites (of $e_g$ character), as shown in panels (a) and (b), and the ones mostly pointing away from the O sites (of $t_{2g}$ character), as shown in panels (c)–(e). Based on the crystal-field splitting, it can be realized that the two MLWFs pointing toward the O sites are associated with the empty Co 3$d$ states (above $E_F$), and the three MLWFs pointing away from the O sites are associated with the occupied Co 3$d$ states (below $E_F$). As to the O 2$p$ MLWFs, two of them overlap with La sites, as shown in panels (f) and (g). The remaining one shown in panel (h) points toward Co site, but it avoids forming Co-O bonding state, as can be observed from the concave on its lobe.

In the LDA+$U$ case (Fig. 10), since an energy gap is opened, the empty Co 3$d$ MLWFs are directly constructed from the conduction band, and the occupied MLWFs are directly constructed from the valence band. The two empty Co 3$d$ MLWFs plotted in panels (a) and (b) point toward the O sites, as can be expected, and they show Co-O antibonding character. The corresponding Co-O bonding states can be observed in the two O 2$p$ MLWFs that point toward Co sites in panels (g) and (h). These are not observed in LDA. The formation of bonding and antibonding states between Co and O sites is consistent with the fact that a gap is opened between the O 2$p$ band (on the top of the valence band) and $e_g$ band (at the bottom of the conduction band), as shown in Fig. 7, and the fact that PDOS peaks of $e_g$ and O 2$p$ state occur at the same energy. On the contrary, the MLWFs in LDA do not show evident Co-O bonding or antibonding character. This is consistent with the PDOS of $e_g$ and O 2$p$ in LDA, having no peak at the same energy (see Fig. 6). Also, the distinction between the empty and occupied Co 3$d$ MLWFs in LDA+$U$ is more evident than in LDA. In LDA, the occupied MLWFs still somewhat lie in between Co and O sites, as can be seen in Figs. 9(d) and 9(e). This part of the MLWF has finite projection on the $d_{3z^2-r^2}$ and $d_{x^2-y^2}$ states that are used for PDOS calculation. This is the reason why LDA has finite PDOS for $e_g$ states, even though Co-O bond-

ing is not observed. Another difference is that in LDA+$U$, only one of the O $2p$ MLWFs overlap with La, as shown in Fig. 10(f), while in LDA there are two, as mentioned previously.

The different Co-O bonding states and La-O overlapping between LDA and LDA+$U$ are consistent with their different structural parameters. In the LDA case, the greater La-O overlapping shortens not only the La-O distance but also the distance between La and Co. In other words, the rhombohedral unit cell shrinks along the [111] direction, which causes smaller lattice constant $a$ and greater rhombohedral angle $\alpha$, as can be seen in Table II. In LDA+$U$, Co-O bonding states are formed, consistent with its shorter Co-O distance. With longer La-O distance and shorter Co-O distance, LDA+$U$ gives a greater tolerance factor (closer to 1), consistent with its Co-O-Co and O-Co-O angles being closer to cubic perovskite than the LDA results. As a consequence, the structural parameters obtained by using LDA+$U$ agree better with the experimental result, which is less distorted with respect to cubic perovskite.

It is worthy to mention that for a specified unit-cell volume $V$, the atomic structures of the LS $LaCoO_3$ given by the several choices of Hubbard $U$ in this paper are nearly the same, as can be seen in Figs. 11 and 12, where lattice constant $a$, rhombohedral angle $\alpha$, and Co-O distance and bond angles are plotted as functions of $V$. The curves given by fixed $U$ and volume-dependent $U_o$ and $U_{sc}$ coincide. This means that as long as a Hubbard $U$ is applied, even if the structurally consistent $U_{sc}$ is not, a less distorted perovskite structure can be obtained, and thus agree with experiment better than LDA results. Also, the improvement of electronic structure at a given volume can be made by applying any one of the Hubbard $U$ being considered. These $U$ values give almost identical PDOS (not shown). The advantage of using structurally consistent $U_{sc}$ is a more accurate estimate of pressure. This is the reason why when the structural properties are plotted with pressure, $U_{sc}$ gives the most accurate results.

Two sets of experimental data are also plotted as a reference. The green triangles are the data taken at $T=298$ K and $10^{-4}<P<8$ GPa.[24] They are plotted versus the volumes corresponding to the pressure at which the measurement is made. The orange squares are taken under $P=10^{-4}$ GPa and $5<T<1000$ K.[16] They are plotted versus the volumes corresponding to the temperature at which the measurement is made. Again, we can see that the structure of LS $LaCoO_3$ behaves differently from the spin-excited $LaCoO_3$. The small differences between the calculation and the $T=5$ K measurements are expected to be reduced with the inclusion of zero-point motion.

## IV. CONCLUSION

In this paper, zero-temperature atomic and electronic structures of low-spin $LaCoO_3$ at different pressures are presented. Several methods are used, including LDA, GGA, and LDA+$U$ with different choices of Hubbard $U$. The results given by LDA+$U$ with structurally consistent Hubbard $U$, $U_{sc}$, agree with experimental results better than other methods.

In the LDA case, La-O overlapping is greater, and the $2p$ electrons of oxygen are less bonded with cobalt. By applying the Hubbard $U$, the occupied $3d$ states of cobalt become more $t_{2g}$-like, evident bonding and antibonding states of Co $e_g$ and O $2p$ characters are formed, and the $LaCoO_3$ lattice is less distorted with respect to cubic perovskite structure. Therefore, the structural parameters obtained from LDA+$U$ at a given volume are closer to experimental results. When the structurally consistent $U_{sc}$ is employed, pressures are estimated more accurately, and a better equation of states (volume-pressure relation) can be obtained.

It is also observed that the structural parameters of LS $LaCoO_3$ behave differently from the experimental data when the lattice is expanded or compressed. This is mainly because $LaCoO_3$ is no longer in pure low-spin state under these conditions.

## ACKNOWLEDGMENTS

This work was supported primarily by the MRSEC Program of the National Science Foundation under Grants No. DMR-0212302 and No. DMR-0819885 and partially by the NSF/ITR program through the University of Texas (ITAMIT). We thank Chris Leighton for stimulating our interest on this problem and for helpful discussions. R.W. acknowledges grant NSF/ATM under Contract No. 0428774(VLab), the Humboldt Foundation, and the hospitality of Bjoern Winkler and Goethe University, Frankfurt, during the final stages of preparation of this paper. Computations were performed at the Minnesota Supercomputer Institute (MSI).

[1] M. Imada, A. Fujimori, and Y. Tokura, Rev. Mod. Phys. **70**, 1039 (1998) and references therein.

[2] J. B. Goodenough, *Localized to Itinerant Electronic Transition in Perovskite Oxides* (Springer, New York, 2001) (and references therein).

[3] C. N. R. Rao, Md. Motin Seikh, and C. Narayana, Top. Curr. Chem. **234**, 1 (2004) and references therein.

[4] M. A. Korotin, S. Yu. Ezhov, I. V. Solovyev, V. I. Anisimov, D. I. Khomskii, and G. A. Sawatzky, Phys. Rev. B **54**, 5309 (1996).

[5] Z. Yang, Z. Huang, L. Ye, and X. Xie, Phys. Rev. B **60**, 15674 (1999).

[6] I. A. Nekrasov, S. V. Streltsov, M. A. Korotin, and V. I. Anisimov, Phys. Rev. B **68**, 235113 (2003).

[7] K. Knížek, P. Novák, and Z. Jirák, Phys. Rev. B **71**, 054420 (2005).

[8] K. Knížek, Z. Jirák, J. Hejtmánek, and P. Novák, J. Phys.: Condens. Matter **18**, 3285 (2006).

[9] S. K. Pandey, Ashwani Kumar, S. Patil, V. R. R. Medicherla, R. S. Singh, K. Maiti, D. Prabhakaran, A. T. Boothroyd, and A. V. Pimpale, Phys. Rev. B **77**, 045123 (2008).

[10] S. Yamaguchi, Y. Okimoto, and Y. Tokura, Phys. Rev. B **55**, R8666 (1997).
[11] K. Asai, A. Yoneda, O. Yokokura, J. M. Tranquada, G. Shirane, and K. Kohn, J. Phys. Soc. Jpn. **67**, 290 (1998).
[12] Y. Tokura, Y. Okimoto, S. Yamaguchi, H. Taniguchi, T. Kimura, and H. Takagi, Phys. Rev. B **58**, R1699 (1998).
[13] S. Murata, S. Isida, M. Suzuki, Y. Kobayashi, K. Asai, and K. Kohn, Physica B **263-264**, 647 (1999).
[14] S. R. English, J. Wu, and C. Leighton, Phys. Rev. B **65**, 220407(R) (2002).
[15] C. Zobel, M. Kriener, D. Bruns, J. Baier, M. Gruninger, T. Lorenz, P. Reutler, and A. Revcolevschi, Phys. Rev. B **66**, 020402(R) (2002).
[16] P. G. Radaelli and S.-W. Cheong, Phys. Rev. B **66**, 094408 (2002).
[17] G. Maris, Y. Ren, V. Volotchaev, C. Zobel, T. Lorenz, and T. T. M. Palstra, Phys. Rev. B **67**, 224423 (2003).
[18] J.-Q. Yan, J.-S. Zhou, and J. B. Goodenough, Phys. Rev. B **69**, 134409 (2004).
[19] J. Baier, S. Jodlauk, M. Kriener, A. Reichl, C. Zobel, H. Kierspel, A. Freimuth, and T. Lorenz, Phys. Rev. B **71**, 014443 (2005).
[20] M. W. Haverkort, Z. Hu, J. C. Cezar, T. Burnus, H. Hartmann, M. Reuther, C. Zobel, T. Lorenz, A. Tanaka, N. B. Brookes, H. H. Hsieh, H.-J. Lin, C. T. Chen, and L. H. Tjeng, Phys. Rev. Lett. **97**, 176405 (2006).
[21] A. Podlesnyak, S. Streule, J. Mesot, M. Medarde, E. Pomjakushina, K. Conder, A. Tanaka, M. W. Haverkort, and D. I. Khomskii, Phys. Rev. Lett. **97**, 247208 (2006).
[22] M. W. Haverkort, arXiv:cond-mat/0505214 (unpublished).
[23] R. F. Klie, J. C. Zheng, Y. Zhu, M. Varela, J. Wu, and C. Leighton, Phys. Rev. Lett. **99**, 047203 (2007).
[24] T. Vogt, J. A. Hriljac, N. C. Hyatt, and P. Woodward, Phys. Rev. B **67**, 140401(R) (2003).
[25] J.-S. Zhou, J.-Q. Yan, and J. B. Goodenough, Phys. Rev. B **71**, 220103(R) (2005).
[26] G. Vankó, J.-P. Rueff, A. Mattila, Z. Németh, and A. Shukla, Phys. Rev. B **73**, 024424 (2006).
[27] D. P. Kozlenko, N. O. Golosova, Z. Jirak, L. S. Dubrovinsky, B. N. Savenko, M. G. Tucker, Y. Le Godec, and V. P. Glazkov, Phys. Rev. B **75**, 064422 (2007).
[28] S. Yamaguchi, Y. Okimoto, H. Taniguchi, and Y. Tokura, Phys. Rev. B **53**, R2926 (1996).
[29] S. Yamaguchi, Y. Okimoto, and Y. Tokura, Phys. Rev. B **54**, R11022 (1996).
[30] Y. Tokura, Y. Okimoto, S. Yamaguchi, H. Taniguchi, T. Kimura, and H. Takagi, Phys. Rev. B **58**, R1699 (1998).
[31] V. I. Anisimov, F. Aryasetiawan, and A. I. Lichtenstein, J. Phys.: Condens. Matter **9**, 767 (1997).
[32] T. Tsuchiya, R. M. Wentzcovitch, C. R. S. da Silva, and S. de Gironcoli, Phys. Rev. Lett. **96**, 198501 (2006).
[33] M. Cococcioni and S. de Gironcoli, Phys. Rev. B **71**, 035105 (2005).
[34] P. Giannozzi *et al.*, http://www.quantum-espresso.org
[35] D. Vanderbilt, Phys. Rev. B **41**, 7892 (1990).
[36] R. M. Wentzcovitch, J. L. Martins, and G. D. Price, Phys. Rev. Lett. **70**, 3947 (1993).
[37] T. Arima, Y. Tokura, and J. B. Torrance, Phys. Rev. B **48**, 17006 (1993).
[38] A. Chainani, M. Mathew, and D. D. Sarma, Phys. Rev. B **46**, 9976 (1992).
[39] M. Abbate, J. C. Fuggle, A. Fujimori, L. H. Tjeng, C. T. Chen, R. Potze, G. A. Sawatzky, H. Eisaki, and S. Uchida, Phys. Rev. B **47**, 16124 (1993).
[40] T. Saitoh, T. Mizokawa, A. Fujimori, M. Abbate, Y. Takeda, and M. Takano, Phys. Rev. B **55**, 4257 (1997).
[41] N. Marzari and D. Vanderbilt, Phys. Rev. B **56**, 12847 (1997).
[42] I. Souza, N. Marzari, and D. Vanderbilt, Phys. Rev. B **65**, 035109 (2001).
[43] A. A. Mostofi, J. R. Yates, Y.-S. Lee, I. Souza, D. Vanderbilt, and N. Marzari, Comput. Phys. Commun. **178**, 685 (2008).